McCue, Scott W. and Johnpillai, I. Kenneth and Hill, James M. (2005) Symmetry analysis for uniaxial compression of a hypoplastic granular material. *Zeitschrift fur angewandte Mathematik und Physik (ZAMP)* 56(6):pp. 1061-1083.

Symmetry analysis for uniaxial compression of a hypoplastic granular material

Scott W. McCue, I. Kenneth Johnpillai and James M. Hill

School of Mathematics and Applied Statistics
University of Wollongong
Wollongong NSW 2522 Australia

Abstract. A variety of modelling approaches currently exist, and continue to be developed, to describe and predict the diverse behaviours of granular materials. One of the more sophisticated theories is hypoplasticity, which is a stress-rate theory of rational continuum mechanics with a constitutive law expressed in a single tensorial equation. In this paper, a particular version of hypoplasticity, due to Wu [2], is employed to describe a class of one-dimensional granular deformations. By combining the constitutive law with the conservation laws of continuum mechanics, a system of four nonlinear partial differential equations is derived for the axial and lateral stress, the velocity and the void ratio. Under certain restrictions, three of the governing equations may be combined to yield ordinary differential equations, whose solutions can be calculated exactly. Several new analytical results are obtained which are applicable to oedometer testing. In general this approach is not possible, and analytic progress is sought via Lie symmetry analysis. A complete set or "optimal system" of group-invariant solutions is identified using the Olver method, which involves the adjoint representation of the symmetry group on its Lie algebra. Each element in the optimal system is governed by a system of nonlinear ordinary differential equations which in general must be solved numerically. Solutions previously considered in the literature are noted, and their relation to our optimal system identified. Two illustrative examples are examined and the variation of various functions occuring in the physical variables is shown graphically.

Keywords. Granular materials; hypoplasticity; exact solutions; group-invariant solutions; Lie symmetries

1 Introduction

The constitutive modelling of granular materials has proven to be a challenging problem for engineers and applied mathematicians. A relatively new path for this research has produced hypoplasticity, a continuum theory formulated as an alternative to the traditional approaches of plasticity and elastoplasticity, and pioneered by Kolymbas [1] and many co-workers originally based at the University of Karlsruhe. The characterising feature of all hypoplastic theories is that the constitutive law can be written in a single nonlinear tensorial equation for the stress-rate as a function of the stress and the rate-of-deformation tensor, without reference to a yield condition or a flow rule. With hypoplasticity there is no need to decompose deformations into elastic and plastic regimes *a priori*, or to distinguish between loading and unloading, since all these notions are automatically built into the theory, and arise as a consequence. A further property of hypoplasticity is that the governing tensorial equation involves only a small number of material parameters.

The success of hypoplasticity and consequent popularity among researchers and practitioners can be attributed to its elegance, relative simplicity, and that the theory is deeply rooted in experimental fact. However, it is certainly a sophisticated constitutive theory, which results in complicated nonlinear mathematical relations. When combined with the governing equations of continuum mechanics, there is little hope of solving real-life boundary-value problems analytically, and progress is usually made via numerical schemes. As a result, it is often difficult to grasp the underlining mathematical structure of the equations. Here, we shed light on this aspect with the use of Lie point symmetry methods. To a limited extent, this approach has been employed by Hill [3, 4, 5] and Hill and Williams [6] for the particular hypoplastic model, originally proposed by Wu [2]. For uniaxial, axially symmetric and radially symmetric deformations, certain group-invariant solutions to the governing partial differential equations were identified, including some similarity solutions, travelling wave solutions, and hot-spot solutions (solutions for which the stresses become infinite in a finite time). These solutions were used to model compaction problems in one dimension and symmetrical cavity expansion problems in two and three dimensions.

In the present study we extend the work of Hill and Williams [6], who restricted the analysis to one-dimensional deformations and uniaxial compaction. Here, for the same deformations, we use Lie symmetry analysis to consider all possible group-invariant solutions to the governing equations, and classify them into equivalence classes. A set containing a single member from each of these classes is a minimal set or "optimal system" of group-invariant solutions. We show that this optimal system contains the families of solutions considered by Hill and Williams [6], as well as certain new families not previously examined. For each member of the optimal system, we list the corresponding system of nonlinear ordinary differential equations, and in two of the cases we solve the equations numerically to illustrate particular behaviour.

In the following section we give a brief outline of the theory of hypoplasticity, and present the particular version of the theory of Wu [2] which is used here. In Section 3, we list the governing equations for uniaxial deformations of a granular material, which include the hypoplastic constitutive equations in one spatial dimension, as well as the conservation laws of continuum mechanics. Under certain conditions, we may manipulate three of these equations to produce ordinary differential equations, which can be integrated analytically. These calculations lead to exact relations between the axial stress, the lateral stress and the void ratio, and the results are discussed in the context of oedometer tests in Section 4. The symmetry analysis for the full system of nonlinear partial differential equations is detailed in Section 5, where we derive the optimal system of Lie generators. Each generator in this optimal system corresponds to a family of group-invariant solutions, which are considered in varying detail in Section 6. We close in Section 7 with some final remarks.

2 Brief outline of hypoplasticity

The original versions of hypoplasticity involve a constitutive equation of the form

$$\mathring{\boldsymbol{\sigma}} = \mathbf{H}(\boldsymbol{\sigma}, \mathbf{d}), \tag{1}$$

where $\mathbf{H}$ is a tensorial function, $\boldsymbol{\sigma}$ is the Cauchy stress tensor, and $\mathbf{d}$ is the rate-of-deformation tensor (otherwise known as the stretching tensor or the rate-of-strain tensor). The tensor $\overset{\circ}{\boldsymbol{\sigma}}$ is the co-rotational or Jaumann stress rate, defined by

$$\overset{\circ}{\boldsymbol{\sigma}} = \frac{D\boldsymbol{\sigma}}{Dt} + \boldsymbol{\sigma}\boldsymbol{\omega} - \boldsymbol{\omega}\boldsymbol{\sigma},$$

where $\boldsymbol{\omega}$ is the skew-symmetric spin tensor, and the notation D/Dt is used to denote the material time derivative

$$\frac{D}{Dt} = \frac{\partial}{\partial t} + (\mathbf{v} \cdot \boldsymbol{\nabla}). \tag{2}$$

Both $\mathbf{d}$ and $\boldsymbol{\omega}$ can be defined in terms of the velocity vector $\mathbf{v}$ as

$$\mathbf{d} = \tfrac{1}{2}[(\boldsymbol{\nabla}\mathbf{v}) + (\boldsymbol{\nabla}\mathbf{v})^T], \quad \boldsymbol{\omega} = \tfrac{1}{2}[(\boldsymbol{\nabla}\mathbf{v}) - (\boldsymbol{\nabla}\mathbf{v})^T],$$

where the superscript T denotes a transposition.

There are a number of additional restrictions which hypoplasticity imposes on the function $\mathbf{H}$ in (1), and we briefly list them here. First it is assumed that $\mathbf{H}$ is a continuously differentiable function of $\mathbf{d}$, except at $\mathbf{d} = \mathbf{0}$. The theory is to be applied to rate-independent material behaviour, so that $\mathbf{H}$ must be positively homogeneous of the first order in $\mathbf{d}$. Therefore $\mathbf{H}(\boldsymbol{\sigma}, \lambda\mathbf{d}) = \lambda\mathbf{H}(\boldsymbol{\sigma}, \mathbf{d})$, where λ is a positive constant. It is also assumed that $\mathbf{H}$ is homogeneous in $\boldsymbol{\sigma}$, so that the material conforms with Goldscheider's principle [7]. Experiments suggest that this homogeneity can be taken to be of the first order, at least as a first approximation, implying $\mathbf{H}(\lambda\boldsymbol{\sigma}, \mathbf{d}) = \lambda\mathbf{H}(\boldsymbol{\sigma}, \mathbf{d})$. Finally, it is required that the constitutive equation (1) be objective, a condition which is satisfied if $\mathbf{H}$ is chosen according to the representation theorem for isotropic tensor-valued functions of two symmetric tensors (Wang [8]). We note that a full description of the history and development of these ideas can be found in Kolymbas and Wu [9], Kolymbas [10], Wu and Kolymbas [11], and the references therein.

It is common to consider a class of functions $\mathbf{H}$ which can be written as the sum of two terms

$$\mathbf{H}(\boldsymbol{\sigma}, \mathbf{d}) = \mathbf{L}(\boldsymbol{\sigma}, \mathbf{d}) + \mathbf{N}(\boldsymbol{\sigma})||\mathbf{d}||, \tag{3}$$

where $||\mathbf{d}||$ denotes the Euclidean norm $||\mathbf{d}|| = \sqrt{\mathrm{tr}(\mathbf{d}^2)}$. The second term in (3) is non-linear in $\mathbf{d}$, and represents irreversible behaviour of the granular material. The other term

$\mathbf{L}(\boldsymbol{\sigma}, \mathbf{d})$ taken to be linear in $\mathbf{d}$, and represents reversible behaviour. (This representation may be contrasted with hypoelasticity, proposed by Truesdell [12], for which the function $\mathbf{H}$ is linear in $\mathbf{d}$.) There are a number of specific versions of (3). In the present study we choose to use the form

$$\mathbf{H} = C_1 \mathrm{tr}(\boldsymbol{\sigma})\mathbf{d} + C_2 \frac{\mathrm{tr}(\boldsymbol{\sigma}\mathbf{d})}{\mathrm{tr}(\boldsymbol{\sigma})}\boldsymbol{\sigma} + (C_3\boldsymbol{\sigma}^2 + C_4\boldsymbol{\sigma}^{*2})\frac{||\mathbf{d}||}{\mathrm{tr}(\boldsymbol{\sigma})}, \tag{4}$$

proposed by Wu [2]. Here $\boldsymbol{\sigma}^*$ denotes the deviatoric stress tensor, defined by $\boldsymbol{\sigma}^* = \boldsymbol{\sigma} - \mathrm{tr}(\boldsymbol{\sigma})\mathbf{I}/3$, where $\mathbf{I}$ is the unit tensor. The four constants C_1, C_2, C_3 and C_4, which depend on the inital void ratio, are dimensionless material parameters, which can be determined with a single triaxial compression test. They are related to the well-known parameters of initial tangential stiffness, initial Poisson ratio, angle of internal friction and angle of dilatancy, as detailed in Wu and Bauer [13]. These authors also show that this model captures the prominent behaviour of granular materials, and as such, will serve the purposes of this study. Typical numerical values for the constants C_1, C_2, C_3 and C_4 are given in Table 1. The first row of data is taken from Wu *et al.* [14], while the rest comes from Wu and Bauer [13].

	C_1	C_2	C_3	C_4
Karlsruhe medium sand	−106.5	−801.5	−797.1	1077.7
Karlsruhe medium sand (loose)	−69.4	−673.1	−655.9	699.6
Karlsruhe medium sand (dense)	−101.2	−962.1	−877.3	1229.2
Undrained Castro sand (loose)	−20.0	−193.2	−193.2	190.0
Undrained Castro sand (dense)	−33.3	−279.2	−279.2	354.5
Erksak medium sand (dense)	−200.0	−1572.5	−1572.5	2583.3
Leighton Buzzard sand (dense)	−73.3	−542.2	−542.2	719.5
Toyoura sand (loose)	−123.3	−1162.5	−1162.5	1494.2
Toyoura sand (dense)	−130.0	−984.9	−984.9	1374.9

Table 1: Typical values for the parameters C_i, $i = 1, \ldots, 4$, in the constitutive equation (4)

We note that while (4) has proven to be an effective constitutive law for granular

materials under many circumstances, it does have has some deficiencies (as do other models of the form (1)), such as the fact that the function $\mathbf{H}$ does not depend explicitly on the void ratio e, but the constants C_i do. Ideally $\mathbf{H}$ would incorporate a dependence of e, and any parameters would be identified for one void ratio e only, and remain constant when e varies. This goal has motivated the research of Wu and Bauer [15], Wu *et al.* [14], Wu [16] and others, who improve on (4) by multiplying the nonlinear terms by a density index, which depends explicitly on the void ratio. Such an approach builds in the concept of a critical state into the constitutive equation. Another example of an extension to (4) has been suggested by Bauer and Wu [17], who also incorporate the effects of cohesion into the model. These additional modifications to the original model reduce the possibility of analytic progress in determining group-invariant solutions, and thus at present we restrict ourselves to the simpler constitutive law (4).

3 Governing equations for uniaxial deformations

We are concerned here with granular deformations in one spatial direction. A Cartesian coordinate system (x, y, z) is introduced so that the x-axis points in the direction of gravity, and it is assumed all physical quantities are independent of the y and z directions. The components of the Cauchy stress tensor $\boldsymbol{\sigma}$ are assumed to be of the form

$$\begin{pmatrix} \sigma_{xx} & \sigma_{xy} & \sigma_{xz} \\ \sigma_{xy} & \sigma_{yy} & \sigma_{xz} \\ \sigma_{xz} & \sigma_{xz} & \sigma_{zz} \end{pmatrix} = \begin{pmatrix} T & 0 & 0 \\ 0 & S & 0 \\ 0 & 0 & S \end{pmatrix},$$

where $T = T(x,t)$ and $S = S(x,t)$, and the component of velocity in the x-direction is denoted by $v = v(x,t)$. It follows that the constitutive equation (4) in component-form becomes

$$\frac{\partial T}{\partial t} + v\frac{\partial T}{\partial x} = \left[C_1(T+2S) + C_2\frac{T^2}{T+2S}\right]\frac{\partial v}{\partial x} + \left[C_3\frac{T^2}{T+2S} + C_4\frac{4(T-S)^2}{9(T+2S)}\right]\left|\frac{\partial v}{\partial x}\right|, \quad (5)$$

$$\frac{\partial S}{\partial t} + v\frac{\partial S}{\partial x} = C_2\frac{ST}{T+2S}\frac{\partial v}{\partial x} + \left[C_3\frac{S^2}{T+2S} + C_4\frac{(T-S)^2}{9(T+2S)}\right]\left|\frac{\partial v}{\partial x}\right|. \quad (6)$$

These two equations are to be supplemented with the usual conservation laws from continuum mechanics. In one dimension, these are mass conservation

$$\frac{\partial e}{\partial t} + v\frac{\partial e}{\partial x} = (1+e)\,\frac{\partial v}{\partial x}, \tag{7}$$

and the conservation of momentum

$$\frac{\partial v}{\partial t} + v\frac{\partial v}{\partial x} = \frac{(1+e)}{\rho_s}\frac{\partial T}{\partial x} + g, \tag{8}$$

where ρ_s is the material density of the grains in the granular material, g is the acceleration due to gravity, and $e = e(x,t)$ is the void ratio. The latter quantity is defined as the ratio of the void volume to the solid volume within the granular material, and in deriving (7)-(8) it has been tacitly assumed that $\rho_s \ll \rho_v$, where ρ_v is the density of the voids.

Hill and Williams [6] considered the above equations in the context of dynamical uniaxial compaction. A blast of air is used to compress moulding sand around a pattern with the intention that the compressed sand is sufficiently strong to allow the pattern to be removed so that molten metal can be poured into the mould. The air pressure impact produces a compaction shock front travelling downwards such that behind the front the sand density and strength are increased. When the shock front reaches either the mould base or the pattern, a second shock front is generated which travels upwards and further compacts the and strengthens the sand. We discuss the relevant group-invariant solution to this problem in Subsection 6.2.

4 Some exact results

4.1 The case $e+1 = E(\xi)$, $S = G(\xi)$ and $T = F(\xi)$

This subsection is concerned with the special case for which e, S and T are of the form

$$e(x,t) + 1 = E(\xi), \quad S(x,t) = G(\xi), \quad T(x,t) = F(\xi), \tag{9}$$

where $\xi = \xi(x,t)$ is some function of x and t. In this case equations (5)-(7) can be rewritten as

$$\frac{DT}{Dt} = \frac{f(\chi)}{1+2\chi} F(\xi) \frac{\partial v}{\partial x}, \tag{10}$$

$$\frac{DS}{Dt} = \frac{g(\chi)}{1+2\chi} F(\xi) \frac{\partial v}{\partial x}, \tag{11}$$

$$\frac{De}{Dt} = E(\xi) \frac{\partial v}{\partial x}, \tag{12}$$

where χ denotes the ratio

$$\chi = \frac{S(x,t)}{T(x,t)} = \frac{G(\xi)}{F(\xi)}, \tag{13}$$

and D/Dt is defined as in (2). The functions f and g used in (10) and (11) each take different forms depending on whether the derivative $\partial v/\partial x$ is positive or negative. For example, f is given by

$$f(\chi) = \begin{cases} C_1(1+2\chi)^2 + (C_2 - C_3) - \frac{4}{9}C_4(1-\chi)^2, & \frac{\partial v}{\partial x} < 0 \\ C_1(1+2\chi)^2 + (C_2 + C_3) + \frac{4}{9}C_4(1-\chi)^2, & \frac{\partial v}{\partial x} > 0. \end{cases}$$

By combining (10), (11) and (13) we arive at

$$\frac{D\chi}{Dt} = \frac{g(\chi) - \chi f(\chi)}{1+2\chi} \frac{\partial v}{\partial x}, \tag{14}$$

where

$$g(\chi) - \chi f(\chi) = \begin{cases} -C_1\chi(1+2\chi)^2 + C_3\chi(1-\chi) - \frac{1}{9}C_4(1-4\chi)(1-\chi)^2, & \frac{\partial v}{\partial x} < 0 \\ -C_1\chi(1+2\chi)^2 - C_3\chi(1-\chi) + \frac{1}{9}C_4(1-4\chi)(1-\chi)^2, & \frac{\partial v}{\partial x} > 0. \end{cases}$$

Dividing (10) by this equation produces the ordinary differential equation

$$\frac{dF}{d\chi} = \frac{f(\chi)}{g(\chi) - \chi f(\chi)} F(\xi), \tag{15}$$

which can readily be solved to give

$$F(\xi) = T_0 \exp\left\{ \int_{\chi_0}^{\chi} \frac{f(\chi')}{g(\chi') - \chi' f(\chi')} \, d\chi' \right\}, \tag{16}$$

where initially $F = T_0$, and $\chi = \chi_0$. The right-hand side of (16) may be evaluated explicitly with the use of partial fractions. Suppose that the roots of

$$g(\chi) - \chi f(\chi) = 0 \tag{17}$$

are $\chi = K_0$, $\alpha \pm i\beta$, where K_0, α and β are real (this is the case for each set of parameter values in Table 1, except for loose undrained Castro sand, where the three roots are real). It thus follows that

$$T = T_0 \left(\frac{\chi_0 - K_0}{\chi - K_0} \right)^m \left(\frac{(\chi_0 - \alpha)^2 + \beta^2}{(\chi - \alpha)^2 + \beta^2} \right)^a \exp \left\{ 2b \arctan \left(\frac{\beta(\chi - \chi_0)}{(\chi_0 - \alpha)(\chi - \alpha) + \beta^2} \right) \right\}, \tag{18}$$

where for $\partial v / \partial x < 0$ the real constants m, a and b are given by

$$m = \frac{K_0^2(36C_1 - 4C_4) + K_0(36C_1 + 8C_4) + 9C_1 + 9C_2 - 9C_3 - 4C_4}{3K_0^2(36C_1 - 4C_4) + 2K_0(36C_1 + 9C_3 + 9C_4) + 9C_1 - 9C_3 - 6C_4},$$

$$a + ib = \frac{(\alpha + i\beta)^2(36C_1 - 4C_4) + (\alpha + i\beta)(36C_1 + 8C_4) + 9C_1 + 9C_2 - 9C_3 - 4C_4}{3(\alpha + i\beta)^2(36C_1 - 4C_4) + 2(\alpha + i\beta)(36C_1 + 9C_3 + 9C_4) + 9C_1 - 9C_3 - 6C_4}.$$

There are analogous results for m, a and b for $\partial v / \partial x > 0$, but we omit the details.

In a similar way, equations (12) and (14) combine to yield

$$\frac{dE}{d\chi} = \frac{1 + 2\chi}{g(\chi) - \chi f(\chi)} E(\xi),$$

which can be integrated to give

$$\begin{aligned} \frac{1 + e}{1 + e_0} &= \exp \left\{ \int_{\chi_0}^{\chi} \frac{1 + 2\chi'}{g(\chi') - \chi' f(\chi')} \, d\chi' \right\} \\ &= \left(\frac{\chi_0 - K_0}{\chi - K_0} \right)^n \left(\frac{(\chi_0 - \alpha)^2 + \beta^2}{(\chi - \alpha)^2 + \beta^2} \right)^c \exp \left\{ 2d \arctan \left(\frac{\beta(\chi - \chi_0)}{(\chi_0 - \alpha)(\chi - \alpha) + \beta^2} \right) \right\}, \end{aligned} \tag{19}$$

where for $\partial v / \partial x < 0$ the real constants n, c and d are given by

$$n = \frac{9(1 + 2K_0)}{3K_0^2(36C_1 - 4C_4) + 2K_0(36C_1 + 9C_3 + 9C_4) + 9C_1 - 9C_3 - 6C_4},$$

$$c + id = \frac{9 + 18(\alpha + i\beta)}{3(\alpha + i\beta)^2(36C_1 - 4C_4) + 2(\alpha + i\beta)(36C_1 + 9C_3 + 9C_4) + 9C_1 - 9C_3 - 6C_4},$$

and K_0 and $\alpha \pm i\beta$ are the roots of (17) (again, similar results for n, c and d hold when $\partial v / \partial x > 0$).

Figure 1 shows some trajectories in (T, S) space for the case in which (9) holds under the further assumption that $\partial v / \partial x < 0$. Here we have used the values $C_1 = -106.5$, $C_2 = -801.5$, $C_3 = -797.1$ and $C_4 = 1077.7$, which are for Karlsruhe medium sand (see Table 1). From top to bottom, the solid curves in this figure are for the initial values

$\chi_0 = S_0/T_0 = 2$, 1 and 1/6. The dashed curve is the straight line $S = K_0 T$, where K_0 is the real root of (17) with $\partial v/\partial x < 0$. Note that these curves have been drawn using equation (18), and do not come from integrating (5)-(6) explicitly with respect to time t. We should also mention that the results of this subsection are independent of $|\partial v/\partial x|$, which is a well-known consequence of rate-independence.

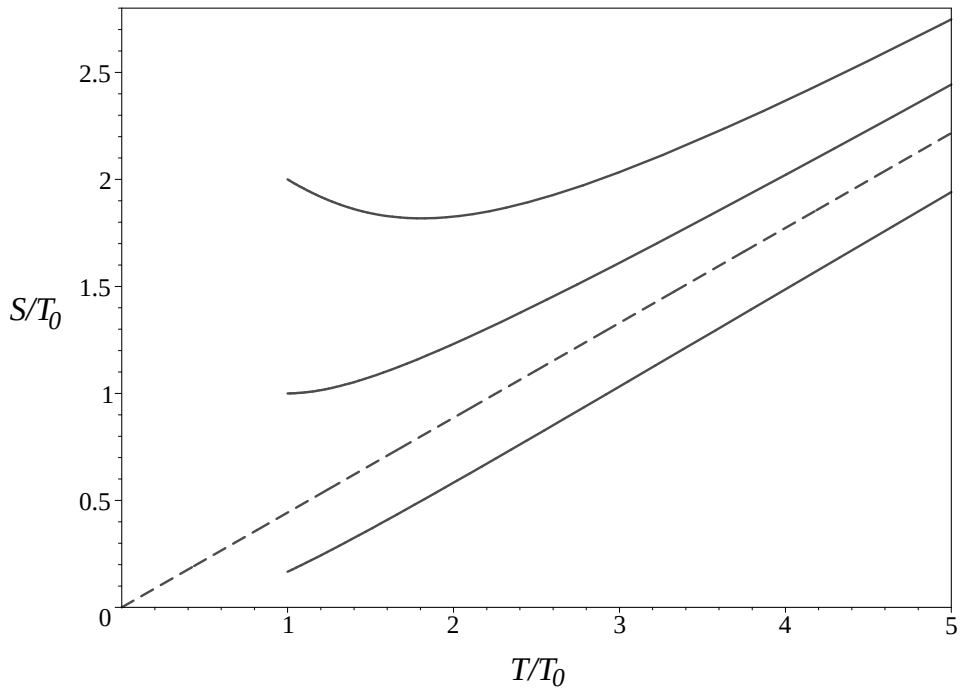

Figure 1: Stress paths resulting from an oedometer test. The solid curves are for $\chi_0 = 1/6$, 1 and 2, while the dashed curve is for $\chi_0 = K_0$. In all cases $C_1 = -106.5$, $C_2 = -801.5$, $C_3 = -797.1$ and $C_4 = 1077.7$.

4.2 Results for oedometer tests

An important uniaxial deformation occurs when granular materials are subject to oedometer tests. During these tests, sometimes referred to as one-dimensional compression tests, a stress T is applied in a vertical axis, but movement in the lateral direction is prevented. The lateral stress S and the axial strain ε are measured as functions of T. A key point is that the deformation is assumed to be homogeneous, so that $e = e(t)$,

$S = S(t)$ and $T = T(t)$, and thus (9) and the analysis of Subsection 4.1 holds. We can therefore think of the curves in Figure 1 as describing oedometer tests under loading.

In oedometer tests, it is found that, regardless of the initial values of the stresses, the curves in stress space approach the line $S = K_0 T$ asymptotically for large T. Here the special constant K_0 for $\partial v/\partial x < 0$ is referred to by engineers as the coefficient of lateral stress at rest. The point $\chi = K_0$ is a fixed point of (14), which means that if the relationship $S/T = K_0$ holds initially, then it holds throughout the deformation. For large T/T_0 we may invert (18) to give the asymptotic behaviour

$$S/T_0 = K_0(T/T_0) + \frac{\lambda(\chi_0 - K_0)}{(T/T_0)^{(1-m)/m}} + O\left(\frac{1}{(T/T_0)^{(2-m)/m}}\right) \quad \text{as} \quad T/T_0 \to \infty, \tag{20}$$

where λ is a constant given by

$$\lambda = \left(\frac{(\chi_0 - \alpha)^2 + \beta^2}{(K_0 - \alpha)^2 + \beta^2}\right)^{A/m} \exp\left\{\frac{2B}{m} \arctan\left(\frac{\beta(K_0 - \chi_0)}{(\chi_0 - \alpha)(K_0 - \alpha) + \beta^2}\right)\right\}.$$

It is clear from (20) that, provided $0 < m < 1$, the predicted behaviour for large T/T_0 from the hypoplastic theory is consistent with experimental observations. For the set of material parameters used to draw Figure 1, the computed value of m is 0.77 and therefore $(1 - m)/m = 0.30$. It follows that the stress paths approach the line $S = K_0 T$ slowly as T/T_0 increases, which is evident from Figure 1.

The curve for $\chi_0 = 2$ in Figure 1 has the feature that as the axial stress T/T_0 is increased from 1, the measured lateral stress S/T_0 decreases at first, and then increases, approaching the line $S/T = K_0$ as $T \to \infty$. This feature is is evident for all values of χ_0 greater than χ_L, where χ_L is the positive root of

$$9C_2\chi - 9C_3\chi^2 - C_4(1 - \chi)^2 = 0,$$

which comes from forcing $dS/dT = 0$. For the set of material parameters used in Figure 1, we have $\chi_L = 1.0055$. It would be interesting to see whether this behaviour could be observed in experiments.

A characteristic of hypoplasticity is its ability to describe the anelastic behaviour of granular materials. This is possible because of the inclusion of the nonlinear term $||\mathbf{d}||$ in (4), which leads to $|\partial v/\partial x|$ appearing in (5)-(6). Figure 2 shows a stress path for

$\partial v/\partial x < 0$ with $\chi_0 = S_0/T_0 = 1$. This is the bottom solid curve, and represents loading in an oedometer test (this curve is also given in Figure 1). When $T/T_0 = 10.47$, the material is unloaded with $\partial v/\partial x > 0$, and this behaviour is described by the top solid curve. The trajectories for loading ($\partial v/\partial x < 0$) and unloading ($\partial v/\partial x > 0$) are different, illustrating the anelastic behaviour of granular materials. The dotted curve in Figure 2 is the same as the dotted curve in Figure 1, and is included for reference.

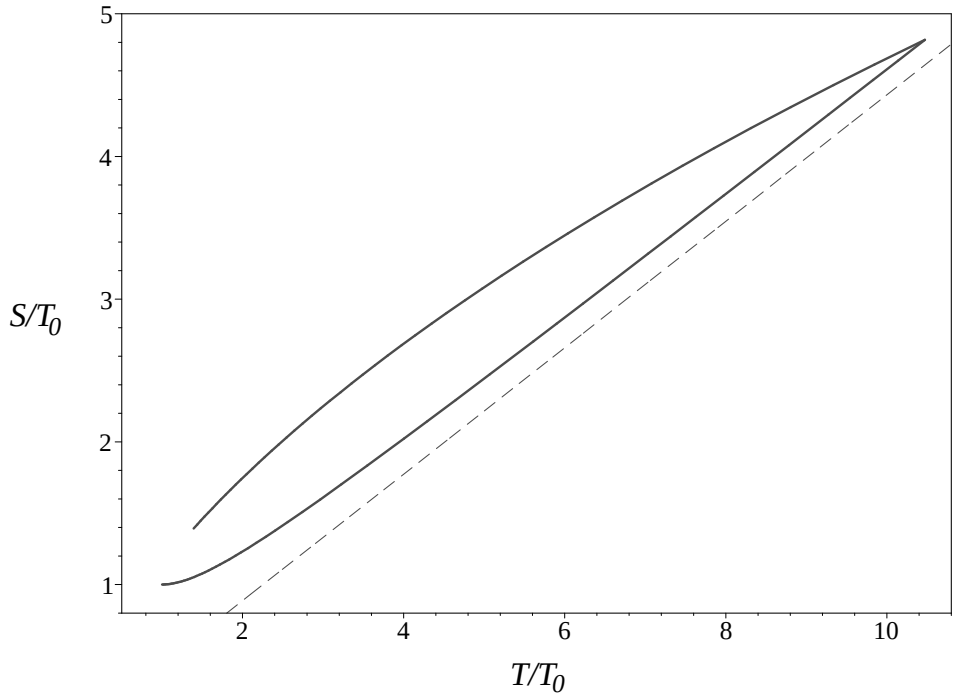

Figure 2: Stress paths for loading (bottom solid curve) and unloading (top solid curve) in an oedometer test, where initially $S_0/T_0 = 1$. The constants C_1, C_2, C_3 and C_4 take the same values as in Figure 1.

In Figure 3 we present the relationship between the void ratio e and the applied stress T/T_0, where the initial void ratio is given by $e_0 = 0.5$. Here the top curve is for loading and the bottom curve for unloading. Again it is clear that these curves differ, demonstrating the ability of this constitutive theory to predict plastic behaviour.

While Figures 1-3 have been described in the context of oedometer tests, it should be understood that they are valid provided (9) holds. Other families of solutions which

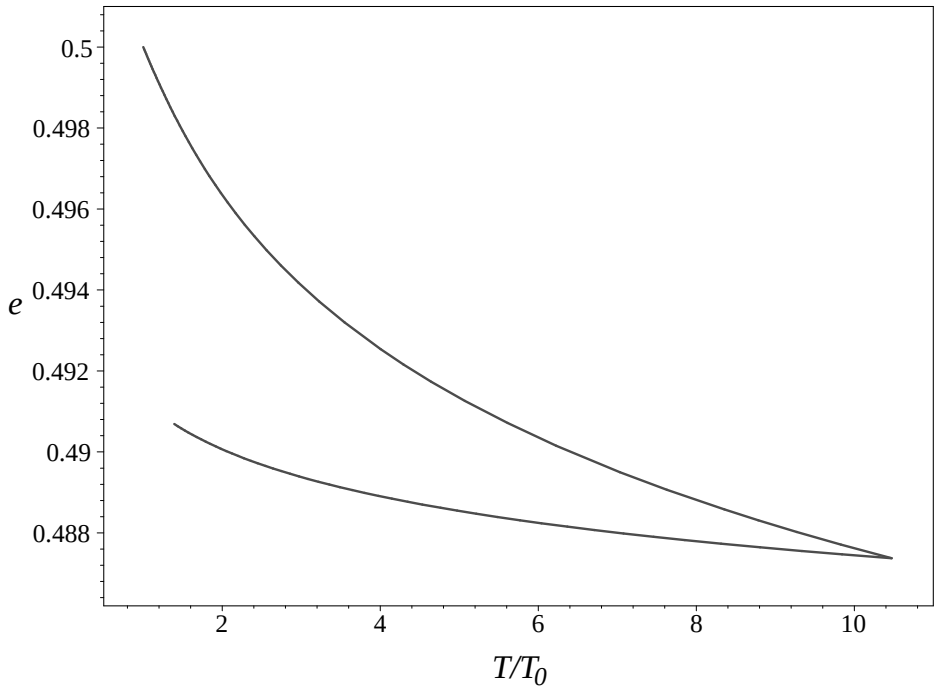

Figure 3: The dependence of the void ratio e on the axial stress T for an oedometer test. The top curve is for loading and the bottom curve is for unloading. The constants C_1, C_2, C_3 and C_4 take the same values as in Figure 1, and initially $S_0/T_0 = 1$ and $e_0 = 0.5$.

are of the form (9) are described later in the paper. For oedometer tests with $e = e(t)$, $S = S(t)$ and $T = T(t)$ we may go further. From (7) or (12) we see that $\partial v/\partial x$ is a function of t alone, which means we may integrate (14) directly to give

$$\varepsilon = \int_{t_0}^{t} \frac{\partial v}{\partial x}\, dt' = \int_{\chi_0}^{\chi} \frac{1 + 2\chi'}{g(\chi') - \chi' f(\chi')}\, d\chi' = \log\left(\frac{1+e}{1+e_0}\right),$$

where ε is the axial strain. We have therefore derived exact relationships between the two stresses S and T, the void ratio e and the axial strain ε.

It should be mentioned that plots similar to those drawn in Figures 1-3 are presented in Wu and Bauer [13] and Wu *et al* [14], who use the same hypoplastic equation (4). These authors also include experimental results in their figures, which are in close agreement with the numerical predictions. We emphasise that all the data in Figures 1-3 are computed via exact results such as (18) and (19). They are *not* found by setting the left-hand sides of (5) and (6) to be dT/dt and dS/dt respectively, arbitrarily choosing negative values

of $\partial v/\partial x$ for loading and positive values for unloading, and then treating (5) and (6) as coupled ordinary differential equations with the dependent variable t, which is the standard practice. In fact, conservation of momentum (8) predicts that the velocity fields for oedometer tests are not arbitrary, but are of the form

$$v(x,t) = \frac{1}{t+k_1}\left(x + \tfrac{1}{2}gt^2 + gk_1k_2t + k_2\right), \tag{21}$$

with the axial strain given by

$$\varepsilon(t) = \log\left(\frac{t+k_1}{t_0+k_1}\right),$$

where k_1 and k_2 are constants, both of which appear not to have been identified in the literature.

5 Lie point symmetry analysis

5.1 Symmetry algebra of (5)-(8)

On using the algebraic package DIMSYM, we find the system of equations (5)-(8) admits a 6-parameter Lie transformation group with the 6 associated linearly independent operators

$$\Gamma_1 = \frac{\partial}{\partial x}, \quad \Gamma_2 = \frac{\partial}{\partial t}, \quad \Gamma_3 = t\frac{\partial}{\partial x} + \frac{\partial}{\partial v}, \quad \Gamma_4 = T\frac{\partial}{\partial T} + S\frac{\partial}{\partial S} - (1+e)\frac{\partial}{\partial e}$$
$$\Gamma_5 = t\frac{\partial}{\partial t} + gt^2\frac{\partial}{\partial x} + (2gt - v)\frac{\partial}{\partial v} - 2(1+e)\frac{\partial}{\partial e}, \quad \Gamma_6 = t\frac{\partial}{\partial t} + (x + \tfrac{1}{2}gt^2)\frac{\partial}{\partial x} + gt\frac{\partial}{\partial v}. \tag{22}$$

For any linear combination of these operators we may determine five invariants of the particular transformation group and hence derive functional forms for the four dependent variables T, S, v and e. There are infinitely many of these linear combinations, so we seek to classify the set of all functional forms into families whose members are all equivalent to each other.

The operators in (22) form a basis for the Lie algebra corresponding to (5)-(8). Of course this basis is not unique, and so while Hill and Williams [6] present a different basis for the Lie algebra (in fact they use two different bases, one for $g \neq 0$, and one for $g = 0$), it can easily be shown that each basis spans the same algebra.

5.2 Optimal system of generators

We define a relation between two invariant solutions to hold true if the first one can be mapped to the other by applying a transformation group generated by a linear combination of the operators in (22). Since these mappings are reflexive, symmetric and transitive, the relation is an equivalence relation, which induces a natural partition on the set of all group invariant solutions into equivalence classes. We need only present one solution from each equivalence class, as the rest may be found by applying appropriate group symmetries; a complete set of such solutions is referred to as an "optimal system" of group invariant solutions.

The problem of deriving an optimal system of group invariant solutions is equivalent to finding an optimal system of generators (or subalgebras spanned by these operators). The method used here is that given by Olver [18], which basically consists of taking linear combinations of the generators in (22), and reducing them to their simplest equivalent form by applying carefully chosen adjoint transformations

$$\mathrm{Ad}(\exp(\epsilon\Gamma_i))\Gamma_j = \Gamma_j - \epsilon[\Gamma_i, \Gamma_j] + \frac{1}{2}\epsilon^2[\Gamma_i, [\Gamma_i, \Gamma_j]] - \ldots.$$

Here $[\Gamma_i, \Gamma_j]$ is the usual commutator, given by

$$[\Gamma_i, \Gamma_j] = \Gamma_i\Gamma_j - \Gamma_j\Gamma_i;$$

the list of adjoint operators is shown in Table 2. For brevity we omit the details, and just state the result that an optimal system of generators is

$$\{\Gamma_2 + \alpha\Gamma_3 + \beta\Gamma_4, \quad \Gamma_6 + \alpha\Gamma_4 + \beta\Gamma_5, \quad \Gamma_6 - \Gamma_5 + \alpha\Gamma_4 + \beta\Gamma_2 \ (\beta \neq 0), \quad \Gamma_6 + \alpha\Gamma_4 \pm \Gamma_3,$$
$$\Gamma_5 + \alpha\Gamma_4 + \beta\Gamma_1, \quad \Gamma_3 + \alpha\Gamma_4, \quad \Gamma_1 + \alpha\Gamma_4, \quad \Gamma_4\}, \tag{23}$$

where α and β denote arbitrary constants.

6 Complete set of group-invariant solutions

For each of the generators in (23) it is straightforward to derive the corresponding functional forms. Again, the reader is referred to Olver [18], or any standard text on Lie

	Γ_1	Γ_2	Γ_3	Γ_4	Γ_5	Γ_6
Γ_1	Γ_1	Γ_2	Γ_3	Γ_4	Γ_5	$\Gamma_6 - \epsilon\Gamma_1$
Γ_2	Γ_1	Γ_2	$\Gamma_3 - \epsilon\Gamma_1$	Γ_4	$\Gamma_5 - \epsilon(\Gamma_2 + 2g\Gamma_3) + \epsilon^2 g\Gamma_1$	$\Gamma_6 - \epsilon(\Gamma_2 + g\Gamma_3) + \frac{1}{2}\epsilon^2 g\Gamma_1$
Γ_3	Γ_1	$\Gamma_2 + \epsilon\Gamma_1$	Γ_3	Γ_4	$\Gamma_5 + \epsilon\Gamma_3$	Γ_6
Γ_4	Γ_1	Γ_2	Γ_3	Γ_4	Γ_5	Γ_6
Γ_5	Γ_1	$e^{\epsilon}\Gamma_2 + g(e^{\epsilon} - e^{-\epsilon})\Gamma_3$	$e^{-\epsilon}\Gamma_3$	Γ_4	Γ_5	Γ_6
Γ_6	$e^{\epsilon}\Gamma_1$	$e^{\epsilon}\Gamma_2 + g(e^{\epsilon} - 1)\Gamma_3$	Γ_3	Γ_4	Γ_5	Γ_6

Table 2: Table of adjoint operators. The (i, j)th entry is $\mathrm{Ad}(\exp(\epsilon\Gamma_i))\Gamma_j$, where the Γ_i are given by (22).

symmetry methods applied to differential equations. We note that Γ_4 does not correspond to any group-invariant solution, so there are seven families of functional forms in our optimal system.

In this section we consider each of the seven families of functional forms, and present the associated system of ordinary differential equations which govern their solution. Families 1 and 2 include solutions examined previously in Hill and Williams [6] at least implicitly; the connection between these families and elements of our optimal system is explained below. The remainder of the solution families given are new, and two illustrative examples of numerical solutions are given.

6.1 Family 1 and travelling wave solutions

The functional forms corresponding to the operator $\Gamma_2 + \alpha\Gamma_3 + \beta\Gamma_4$ in (23) are

$$e(x,t) + 1 = e^{-\beta t}E(\xi), \quad v(x,t) = \alpha t + H(\xi),$$

$$S(x,t) = e^{\beta t}G(\xi), \quad T(x,t) = e^{\beta t}F(\xi), \tag{24}$$

where E, H, G and F are arbitrary functions of $\xi = x - \frac{1}{2}\alpha t^2$. Upon substitution of these functional forms into (5)-(8), we obtain the system of ordinary differential equations

$$HE' - EH' = \beta E, \tag{25}$$

$$\alpha + HH' = \frac{EF'}{\rho_s} + g, \tag{26}$$

$$(F+2G)(\beta F + HF') = H'\{C_1(F+2G)^2 + (C_2 - C_3)F^2 - (4C_4/9)(F-G)^2\}, \tag{27}$$

$$(F+2G)(\beta G + HG') = H'\{C_2 FG - C_3 G^2 - (C_4/9)(F-G)^2\}, \tag{28}$$

where here $\partial v/\partial x < 0$, and the primes denote differentiation with respect to ξ. The corresponding system for $\partial v/\partial x > 0$ is the same as (25)-(28), except that the negative signs in front of the constants C_3 and C_4 will be positive.

The functional forms (24) can be thought of representing accelerating travelling waves, with speed αt. For $\beta = 0$ we have

$$e(x,t) + 1 = E(\xi), \quad v(x,t) = \alpha t + H(\xi), \quad S(x,t) = G(\xi), \quad T(x,t) = F(\xi),$$

where $\xi = x - \frac{1}{2}\alpha t^2$, and so the exact solutions of Section 4 hold, which means that we know how $e(x,t)$, $T(x,t)$ and $S(x,t)$ depend on each other. However, even in this case the only way to determine the dependence of E, H, G and F on the independent variable ξ is to solve (25)-(28) numerically, since analytic solutions of the full system (25)-(28) are not possible. Figure 4 shows the dependence of E, H, G and F on the invariant ξ for the two values $\beta = 0$ (dashed lines) and $\beta = -0.005\text{s}^{-1}$ (solid lines) with $\alpha = 1\text{m/s}^2$. This solution has been computed with the initial conditions $E(0) = 3/2$, $F(0) = G(0) = -100\text{kN/m}^2$ and $H(0) = 1\text{m/s}$ using the algebraic package MAPLE. The material constants used are for Karlsruhe medium sand, as with the previous figures, with $\rho_s = 0.8\text{g/cm}^3$ and $g = 10\text{m/s}^2$. The curves in Figure 4 are initial profiles for $e+1$, v, S and T. As time evolves, these profiles are adjusted via the exponential terms in (24), and progagate with speed αt.

Hill and Williams [6] considered traditional travelling wave solutions (those for which the wave speed is a constant) of (5)-(8), which corresponds to the symmetry groups generated by the linear combination $\Gamma_2 + k\Gamma_1$ of space and time translational symmetries,

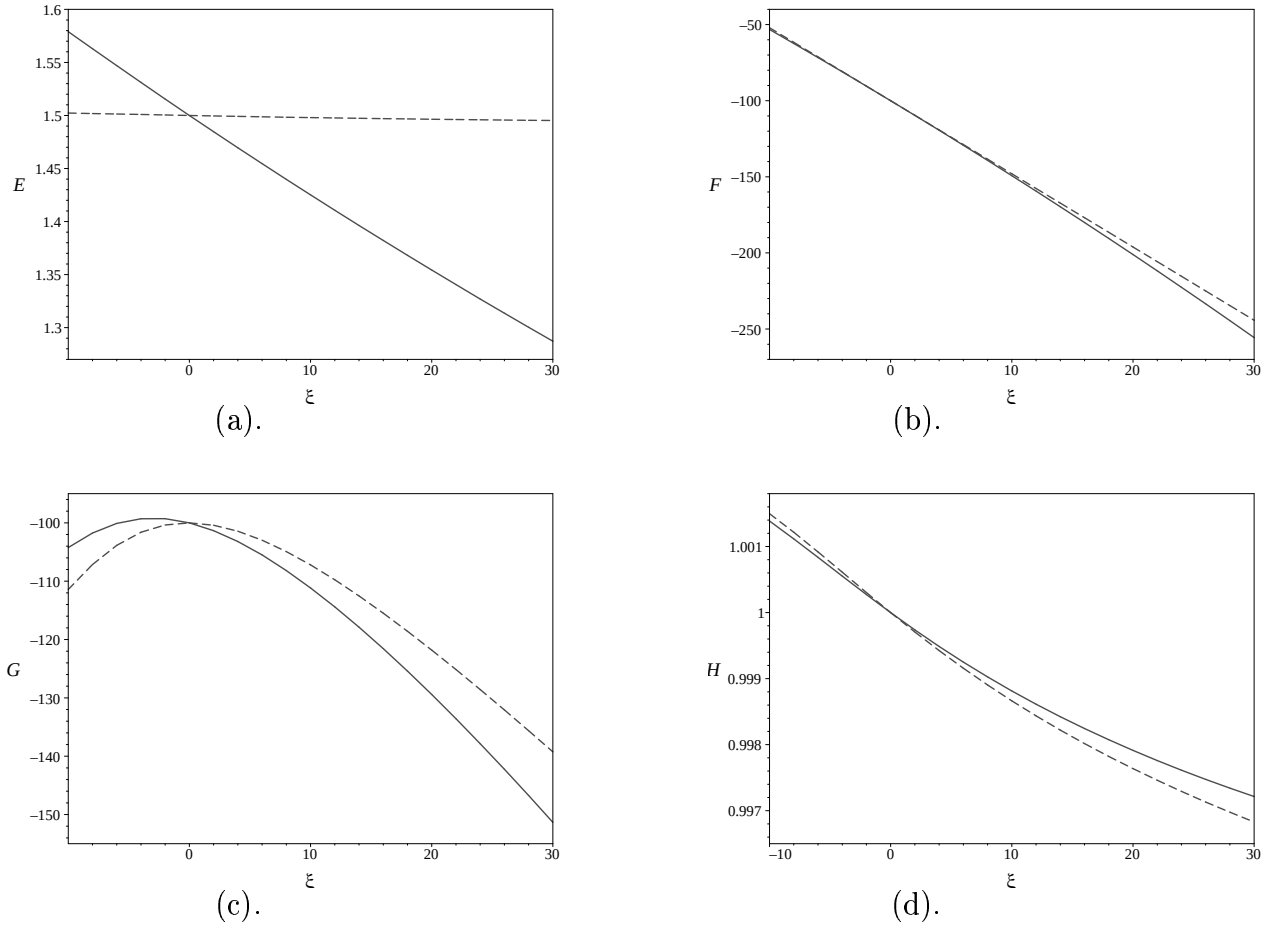

Figure 4: The dependence of E, H, G and F for family 1 on the independent variable ξ is shown for $\beta = 0$ (dashed lines) and $\beta = -0.005\text{s}^{-1}$ (solid lines). In each case $C_1 = -106.5$, $C_2 = -801.5$, $C_3 = -797.1$, $C_4 = 1077.7$, $\alpha = 1\text{m/s}^2$, $\rho_s = 0.8\text{g/cm}^3$ and $g = 10\text{m/s}^2$.

where k is the speed of the wave. We denote these solutions by $e+1 = \tilde{E}(x,t)$, $v = \tilde{H}(x,t)$, $S = \tilde{G}(x,t)$ and $T = \tilde{F}(x,t)$. Referring to Table 2, we find that

$$\text{Ad}(\exp(-k\Gamma_3))(\Gamma_2 + k\Gamma_1) = \Gamma_2,$$

so that the travelling wave solutions $\tilde{E}$, $\tilde{H}$, $\tilde{G}$ and $\tilde{F}$ can be recovered from the stationary solutions $e + 1 = E(x)$, $S = G(x)$, $T = F(x)$, and $v = H(x)$, which are invariant under the group generated by Γ_2 (and correspond to Family 1 with $\alpha = \beta = 0$). The travelling wave solutions

$$e(x,t) = \tilde{E}(x,t) = E(x - kt), \quad v(x,t) = \tilde{H}(x,t) = H(x - kt) + k,$$

$$S(x,t) = \tilde{G}(x,t) = G(x-kt), \text{ and } T(x,t) = \tilde{F}(x,t) = F(x-kt),$$

are therefore derived via invariant transformations of the symmetry Γ_3 with the wave speed k.

6.2 Family 2 and similarity solutions

The functional forms for the operator $\Gamma_6 + \alpha\Gamma_4 + \beta\Gamma_5$ in (23) are

$$e(x,t) + 1 = t^{-\frac{(\alpha+2\beta)}{\beta+1}} E(\xi), \quad v(x,t) = gt + t^{-\frac{\beta}{\beta+1}} H(\xi),$$
$$S(x,t) = t^{\frac{\alpha}{\beta+1}} G(\xi), \quad T(x,t) = t^{\frac{\alpha}{\beta+1}} F(\xi), \tag{29}$$

where E, H, G and F are arbitrary functions of $\xi = t^{-\frac{1}{\beta+1}}(x - \frac{1}{2}gt^2)$, provided $\beta \neq -1$. Upon substitution of these functional forms into (5)-(8), we obtain for $\partial v/\partial x < 0$ the system of ordinary differential equations

$$\begin{aligned}
(\alpha+2\beta)E + \xi E' &= (\beta+1)(HE' - EH'), \\
(\beta H + \xi H') &= (\beta+1)(HH' - EF'/\rho_s), \\
(\alpha F - \xi F' + (\beta+1)HF')(F+2G) &= (\beta+1)H'\{C_1(F+2G)^2 + (C_2 - C_3)F^2 \\
&\quad -(4C_4/9)(F-G)^2\}, \\
(\alpha G - \xi G' + (\beta+1)HG')(F+2G) &= (\beta+1)H'\{C_2FG - C_3G^2 - (C_4/9)(F-G)^2\},
\end{aligned}$$

where the primes denote differentiation with respect to ξ. Again, the system for $\partial v/\partial x > 0$ is obtained by replacing the negative signs in front of the constants C_3 and C_4 by positive ones. For the case $\beta = -1$, the functional forms become

$$e(x,t) + 1 = (x - \tfrac{1}{2}gt^2)^{-(\alpha-2)} E(t), \quad v(x,t) = gt + (x - \tfrac{1}{2}gt^2)H(t),$$
$$S(x,t) = (x - \tfrac{1}{2}gt^2)^{\alpha} G(t), \quad T(x,t) = (x - \tfrac{1}{2}gt^2)^{\alpha} F(t), \tag{30}$$

where now E, H, G and F are governed for $\partial v/\partial x < 0$ by

$$E' = (\alpha - 1)EH, \tag{31}$$
$$(H' + H^2)\rho_s = \alpha EF, \tag{32}$$
$$(F' + \alpha FH)(F+2G) = H\{C_1(F+2G)^2 + (C_2 - C_3)F^2 - (4C_4/9)(F-G)^2\}, \tag{33}$$
$$(G' + \alpha GH)(F+2G) = H\{C_2FG - C_3G^2 - (C_4/9)(F-G)^2\}. \tag{34}$$

The case $\beta = -1$ was discussed in Hill and Williams [6] and the functional forms and corresponding system of ordinary differential equations may be derived from (30) and (31)-(34) if $\alpha = 3/2$, and $g = 0$.

The similarity solutions of Family 2 are invariant under the transformations

$$\bar{x} = \lambda x - (gt^2/2)(\lambda - \lambda^{2(\beta+1)}), \quad 1 + \bar{e} = \lambda^{-(\alpha+2\beta)}(1+e), \quad \bar{S} = \lambda^{\alpha} S, \quad \bar{T} = \lambda^{\alpha} T,$$

$$\bar{v} = v\lambda^{-\beta} + gt(\lambda^{\beta+1} - \lambda^{-\beta}), \quad \bar{t} = \lambda^{\beta+1} t, \tag{35}$$

where λ is a small parameter. In can be seen that by setting $\beta = -1/2$, these transformations are the same as those given by equations (3.10)-(3.11) in Hill and Williams [6]. It must be that $\alpha = 1 - a$, where a is a parameter used in Hill and William's paper.

Hill and Williams [6] investigated similarity solutions under (35) with $\beta = -1/2$. One of these (with $\alpha = -1/2$) was utilized to examine the application to the problem of compaction by air pressure impact. They derived the functional forms

$$e(x,t) + 1 = x^{(1-\alpha)}\mathcal{E}(\tilde{\xi}), \quad v(x,t) = x^{1/2}\mathcal{H}(\tilde{\xi}), \quad S(x,t) = x^{\alpha}\mathcal{G}(\tilde{\xi}), \quad T(x,t) = x^{\alpha}\mathcal{F}(\tilde{\xi}),$$

with $\tilde{\xi}$ defined below, which appear to be different to the functional forms (29) with $\beta = -1/2$, namely

$$e(x,t) + 1 = t^{2(1-\alpha)}E(\xi), \quad v(x,t) = t(g + H(\xi)), \quad S(x,t) = t^{2\alpha}G(\xi), \quad T(x,t) = t^{2\alpha}F(\xi),$$

where $\xi = x/t^2 - g/2$. It should be clear that these different sets of functional forms are equivalent to each other, and in fact the relevant functions are related by

$$E(\xi) = \tilde{\xi}^{1-\alpha}\mathcal{E}(\tilde{\xi}), \quad H(\xi) = \tilde{\xi}^{1/2}\mathcal{H}(\tilde{\xi}) - g, \quad G(\xi) = \tilde{\xi}^{\alpha}\mathcal{G}(\tilde{\xi}), \quad F(\tilde{\xi}) = \tilde{\xi}^{\alpha}\mathcal{F}(\tilde{\xi}), \quad \tilde{\xi} = \xi + g/2.$$

We note that there are many types of solutions from Family 2, other than that those considered by Hill and Williams [6], but we do not investigate these solutions further here.

6.3 Family 3

The operator $\Gamma_6 - \Gamma_5 + \alpha\Gamma_4 + \beta\Gamma_2$ $(\beta \neq 0)$ in (23) yields the functional forms

$$e(x,t) + 1 = e^{-(\alpha-2)t/\beta}E(\xi), \quad v(x,t) = g(t+\beta) + e^{t/\beta}H(\xi),$$

$$S(x,t) = e^{\alpha t/\beta} G(\xi), \quad T(x,t) = e^{\alpha t/\beta} F(\xi),$$

where E, H, G and F are arbitrary functions of $\xi = [x - \frac{1}{2}g((t+\beta)^2 + \beta^2)]e^{-t/\beta}$, noting that the case β zero is embodied in the previous example. For $\partial v/\partial x < 0$ we find that E, H, G and F satisfy the system of ordinary differential equations

$$\begin{aligned}
(\alpha - 2)E + \xi E' &= \beta(HE' - EH'), \\
(1 + \beta H')H - \xi H' &= \frac{\beta E F'}{\rho_s}, \\
\alpha F - \xi F' + \beta H F' &= \frac{\beta H'}{F + 2G}\{C_1(F+2G)^2 + (C_2 - C_3)F^2 - (4C_4/9)(F-G)^2\}, \\
\alpha G - \xi G' + \beta H G' &= \frac{\beta K'}{F + 2G}\{C_2 FG - C_3 G^2 - (C_4/9)(F-G)^2\},
\end{aligned}$$

where the primes indicate the differentiation with respect to ξ. For $\partial v/\partial x > 0$, we arrive at the same equations, with the negative signs in front of the constants C_3 and C_4 changed to positive.

6.4 Family 4

The corresponding functional forms for the operator $\Gamma_6 + \alpha\Gamma_4 \pm \Gamma_3$ in (23) are

$$e(x,t) + 1 = t^{-\alpha} E(\xi), \quad v(x,t) = gt + \log t + H(\xi),$$

$$S(x,t) = t^{\alpha} G(\xi), \quad T(x,t) = t^{\alpha} F(\xi), \tag{36}$$

where E, H, G and F are arbitrary functions of $\xi = te^{-\frac{x}{t} + \frac{1}{2}gt}$. The following system of ordinary differential equations is obtained on substitution of these functional forms into (5)-(8), under the assumption $\partial v/\partial x > 0$:

$$\begin{aligned}
\alpha E + \xi(H - 1 + \log\xi)E' &= \xi E H', \\
1 + (1 - \log\xi - H)\xi H' &= -\frac{\xi E F'}{\rho_s}, \\
(\alpha F + (1 - \log\xi - H)\xi F')(F + 2G) &= -\xi\{C_1(F+2G)^2 + (C_2 + C_3)F^2 \\
&\quad + (4C_4/9)(F-G)^2\}, \\
(\alpha G + (1 - \log\xi - H)\xi G')(F + 2G) &= -\xi\{C_2 FG + C_3 G^2 + (C_4/9)(F-G)^2\}.
\end{aligned} \tag{37}$$

Here the primes denote differentiation with respect to ξ. For $\partial v/\partial x < 0$ the signs of the constants C_3 and C_4 should be changed.

Suppose a piston is being thrusted into a semi-infinite vertical cylinder of material with constant applied stress T_0. Suppose also that at the piston level, which we denote by $x = q(t)$, the lateral stress is S_0 and the void ratio is e_0. Then, providing the piston follows the path

$$q(t) = t\log(t/\gamma) + \tfrac{1}{2}gt^2$$

for some constant γ, then the solution is of the form (36) with $\alpha = 0$. The functions E, H, G and F are determined by the system (37) (with $\alpha = 0$) with the initial conditions $E(\gamma) = e_0 + 1$, $H(\gamma) = 1 - \log\gamma$, $G(\gamma) = S_0$ and $F(\gamma) = T_0$. Furthermore, since $\alpha = 0$, the functional forms satisfy (9), and so the exact results of Section 4.1 apply.

6.5 Family 5

The functional forms for the operator $\Gamma_5 + \alpha\Gamma_4 + \beta\Gamma_1$ in (23) are

$$e(x,t) + 1 = t^{-(\alpha+2)}E(\xi), \quad v(x,t) = gt + \tfrac{1}{t}H(\xi),$$
$$S(x,t) = t^{\alpha}G(\xi), \quad T(x,t) = t^{\alpha}F(\xi), \tag{38}$$

where E, H, G and F are arbitrary functions of $\xi = x - \frac{1}{2}gt^2 - \beta\log t$. By substituting these forms in (5)-(8) we obtain for $\partial v/\partial x < 0$

$$\begin{aligned}
(\alpha+2)E + \beta E' &= HE' - EH', \\
(H-\beta)H' - H &= \frac{EF'}{\rho_s}, \\
(\alpha F + (H-\beta)F')(F+2G) &= H'\{C_1(F+2G)^2 + (C_2 - C_3)F^2 \\
&\quad -(4C_4/9)(F-G)^2\}, \\
(\alpha G + (H-\beta)G')(F+2G) &= H'\{C_2FG - C_3G^2 - (C_4/9)(F-G)^2\},
\end{aligned}$$

where the primes indicate differentiation with respect to ξ, and for $\partial v/\partial x > 0$ we obtain the same equations with the negative signs in front of C_3 and C_4 positive. The functional forms (38) represent some sort of travelling waves with speed $gt + \beta/t$. For $\beta = 0$ these travelling waves' acceleration is due to gravity.

6.6 Family 6

The functional forms corresponding to $\Gamma_3 + \alpha\Gamma_4$ are

$$e(x,t) + 1 = e^{-\alpha x/t}E(t), \quad v(x,t) = \tfrac{x}{t} + H(t),$$

$$S(x,t) = e^{\alpha x/t}G(t), \quad T(x,t) = e^{\alpha x/t}F(t). \tag{39}$$

For time $t < 0$ we have $\partial v/\partial x < 0$, and here E, H, G and F satisfy the coupled system

$$\begin{aligned} tE' &= (1+\alpha H)E, \\ t(H'-g)+H &= \frac{\alpha EF}{\rho_s}, \\ (tF'+\alpha FH)(F+2G) &= \{C_1(F+2G)^2 + (C_2-C_3)F^2 - (4C_4/9)(F-G)^2\} \\ (tG'+\alpha GH)(F+2G) &= \{C_2FG - C_3G^2 - (C_4/9)(F-G)^2\}, \end{aligned} \tag{40}$$

where the primes denote differentiation with respect to t.

Now for $\alpha = 0$ the functional forms (39) are appropriate to describe deformations which occur in oedometer tests, as described in Section 4. In figure 5 we show the dependence of E, H, G and F on t for $\alpha = 0$ (dashed line) and $\alpha = 1\text{sm}^{-1}$ (solid line), found by solving (40) numerically (with MAPLE) subject to the initial conditions $E = 3/2$, $H = 0$, $G = F = -100\text{kN/m}^2$ when $t = -1\text{s}$. This figure simulates loading. We see that the curves for the stresses G and F are almost identical for each value of α, but the functions E and H are sensitive to the choice of α. Recall that from (21) that the function H for $\alpha = 0$ is given exactly by

$$H(t) = \tfrac{1}{2}g(t - 1/t),$$

the form of which is difficult to appreciate from the scale in the figure.

6.7 Family 7

Finally, the functional forms for $\Gamma_1 + \alpha\Gamma_4$ in (23) are

$$e(x,t) + 1 = e^{-\alpha x}E(t), \quad v(x,t) = H(t), \quad S(x,t) = e^{\alpha x}G(t), \quad T(x,t) = e^{\alpha x}F(t).$$

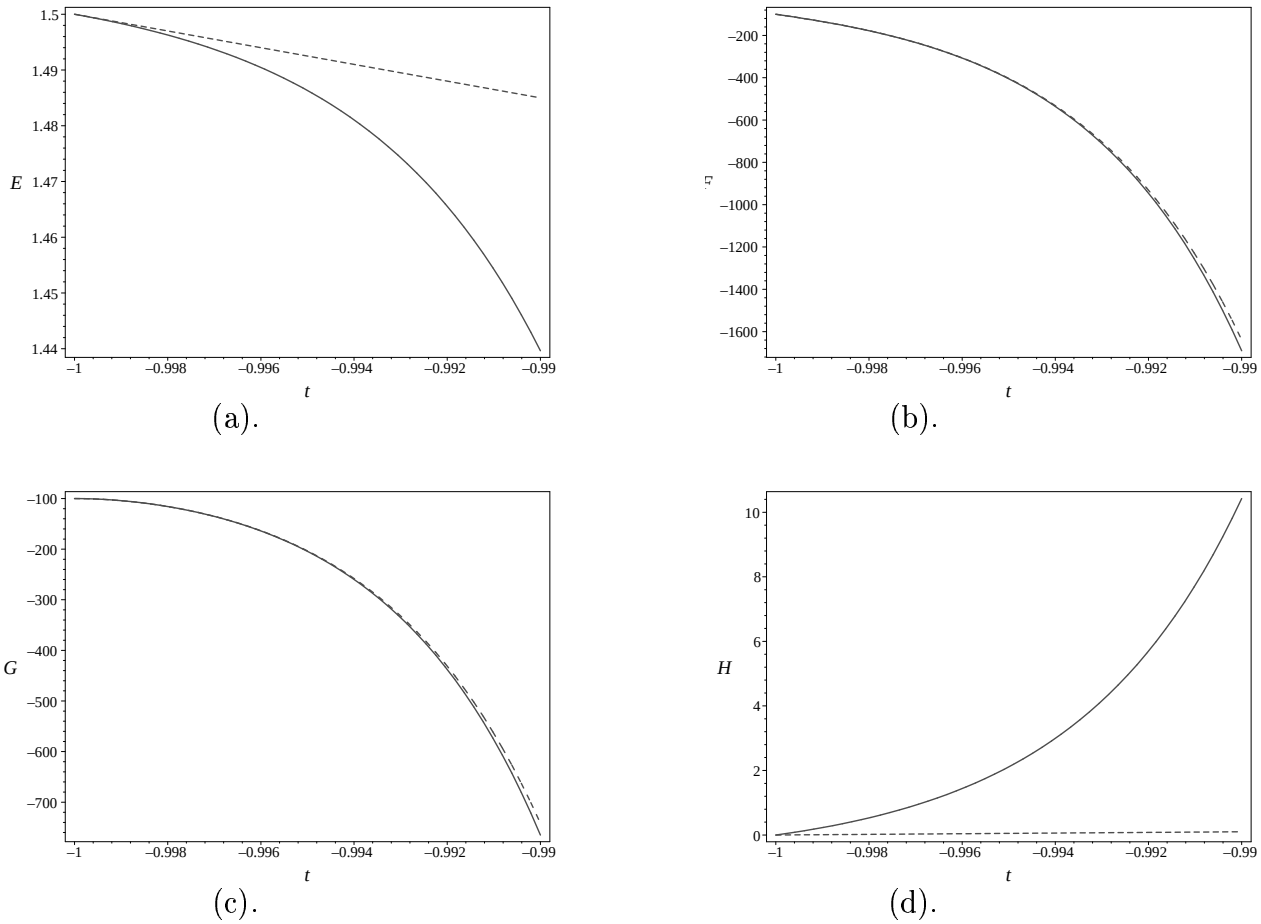

(a). (b). (c). (d).

Figure 5: The dependence of E, H, G and F for family 6 on time t is shown for $\alpha = 0$ (dashed lines) and $\alpha = 1\mathrm{sm}^{-1}$ (solid lines). In each case $C_1 = -106.5$, $C_2 = -801.5$, $C_3 = -797.1$, $C_4 = 1077.7$, $\rho_s = 0.8\mathrm{g/cm}^3$ and $g = 10\mathrm{m/s}^2$.

Here the term $\partial v/\partial x$ vanishes, and so the partial differential equations (5)-(8) reduce considerably to

$$E' = \alpha EH, \quad H' - g = \frac{\alpha EF}{\rho_s}, \quad F' = -\alpha FH, \quad G' = -\alpha GH.$$

In this instance we are able to solve the equations analytically, and the solutions are

$$e(x,t) + 1 = E_1 \exp\{-\alpha(x - \tfrac{1}{2}H_1 t^2 - H_2 t)\}, \quad v(x,t) = H_1 t + H_2,$$

$$S(x,t) = G_1 \exp\{\alpha(x - \tfrac{1}{2}H_1 t^2 - H_2 t)\}, \quad T(x,t) = F_1 \exp\{\alpha(x - \tfrac{1}{2}H_1 t^2 - H_2 t)\},$$

where E_1, F_1, G_1, H_1 are H_2 are constants of integration, with H_1 given by $H_1 = g + \frac{\alpha}{\rho_s} E_1 F_1$.

7 Discussion

Hypoplasticity is a sophisticated continuum theory for granular materials whose constitutive law can be expressed in a single tensorial equation. The theory differs from the classical elastoplasticity theories in that the concept of a yield condition is not used *a priori*, and that there is no need to either decompose deformations into elastic and plastic parts, nor to distinguish explicitly whether the material is experiencing loading or unloading. These characteristics, coupled with the fact that the tensorial equation contains few material parameters, make hypoplasticity an attractive practical constitutive theory for engineers.

Many versions of hypoplasticity have been developed, and at each stage these have been rigorously tested against experimental data, with considerable success. The experiments used are typically in the form of element tests, such as triaxial or simple shearing tests. The reason is that the stress fields resulting from element tests are homogeneous (functions of time only), and the material time derivative of the stresses reduces to a normal derivative. The constitutive equations can then be integrated numerically, without reference to the momentum equation. The particular hypoplastic law used in the present study is due to Wu [2], and has been tested against experimental data in Wu *et al.* [14] and Wu and Bauer [13].

In general, stress fields for deformations of hypoplastic granular materials are not homogeneous, and are described by a nonlinear system of partial differential equations consisting of the hypoplastic equations and the conservation laws of continuum mechanics. These equations are mathematically complicated, with analytic progress unlikely for most realistic boundary-value problems. With this in mind, the goal of Hill and Williams [6] was to examine granular deformations in one spatial deformation, and to derive certain group-invariant solution using Lie symmetry methods. We have extended this work by considering all such group-invariant solutions in a systematic way, and classifying them

into equivalence classes using the established concept of an "optimal system". It has been found that there are seven independent families of group-invariant solutions, in each case governed by ordinary differential equations, which can be easily solved numerically.

For some of the more complicated families considered in Section 6, it is not immediately clear to which physical situation they correspond. An example is family 3, whose similarity-type variable is $\xi = [x - \frac{1}{2}g((t+\beta)^2 + \beta^2)]e^{-t/\beta}$. However, we have derived a variety of travelling wave solutions, such as those of families 1 and 5, which are of interest. A subset of the similarity solutions of family 2 have already been applied to an air compaction problem in Hill and Williams [6], and solutions of family 4 can be applied to a compacting piston problem. Furthermore, in a practical context, solutions in family 6 describe deformations which occur in oedometer tests, which we briefly discuss below. In any event, it is always advantageous to obtain any simplified solutions to nonlinear systems of partial differential equations, and all the solution families considered in this paper could be exploited to test numerical schemes for the full system of partial differential equations.

Finally, we mention that for the class of solutions (9), we have been able to derive several exact results, as presented in Section 4. Within this class are those which describe oedometer tests, which are used by engineers to test theories for granular deformations, including hypoplasticity. In this context these exact results are interesting, since they appear to have been overlooked. The usual practice when dealing with these equations is to assign arbitrary values of $\partial v/\partial x$ for loading and unloading, and then solve the remaining coupled ordinary differential equations numerically. Our exact results are entirely in accord with results obtained in this manner.

Acknowledgements

The authors are grateful to the Australian Research Council for support of this work through a Discovery Project grant.

References

[1] D. Kolymbas, A novel constitutive law for soils, in: *Proceedings of the Second International Conference on Constitutive Laws for Engineering Materials*, Desai CS, ed., Elsevier, Amsterdam, 1987, 319-326.

[2] W. Wu, Hypoplasticity as a mathematical model for the mechanical behaviour of granular materials. *Publication Series of the Institute for Soil and Rock Mechanics No. 129* University of Karlsruhe, Germany 1992.

[3] J. M. Hill, Similarity 'hot-spot' solutions for a hypoplastic granular material. *Proceedings of the Royal Society London A* **456** (2000), 2653-2671.

[4] J. M. Hill, Some symmetrical cavity problems for a hypoplastic granular material. *Quarterly Journal of Mechanics and Applied Mathematics* **53** (2000), 111-135.

[5] J. M. Hill, Dynamical uniaxial and radial flow for hypoplastic granular materials, in: *Bifurcation and Localisation Theory in Geomechanics*, Mühlhaus H. et al., eds., Balkema, 2001, 239-248.

[6] J. M. Hill and K. A. Williams, Dynamical uniaxial compaction of a hypoplastic granular material. *Mechanics of Materials* **32** (2000), 679-691.

[7] M. Goldscheider, Grenzbedingung und Fließregel von Sand. *Mechanics Research Communications* **3** (1976), 463-468.

[8] C. C. Wang, A new representation theorem for isotropic functions, parts I and II. *Journal of Rational Mechanics and Analysis* **36** (1970), 166-223.

[9] D. Kolymbas and W. Wu, Introduction to hypoplasticity, in: *Proceedings of the Modern Approaches to Plasticity*, Kolymbas D., ed., Elsevier, Amsterdam, 1993, 213-223.

[10] D. Kolymbas, *Introduction to Hypoplasticity*. A. A. Balkema, Rotterdam 2000.

[11] W. Wu and D. Kolymbas, Hypoplasticity, then and now, in: *Constitutive Modelling of Granular Materials*, Kolymbas D., ed., Springer Verlag, 2000, 57-105.

[12] C. Truesdell, Hypo-elasticity. *Journal of Rational Mechanics and Analysis* **4** (1965), 83-133.

[13] W. Wu and E. Bauer, A simple hypoplastic constitutive model for sand. *International Journal for Numerical and Analytical Methods in Geomechanics* **18** (1994), 833-862.

[14] W. Wu, E. Bauer and D. Kolymbas, Hypoplastic constitutive model with critical state for granular materials. *Mechanics of Materials* **23** (1996), 45-69.

[15] W. Wu and E. Bauer, A hypoplastic model for barotropy and pyknotropy of granular soils, in: *Proceedings of the Modern Approaches to Plasticity*, Kolymbas D., ed., Elsevier, Amsterdam, 1993, 225-245

[16] W. Wu, On a simple critical state model for sand, in: *Proceedings of the International Symposium on Numerical Methods in Geomechanics*, Balkema: Graz, 1999; 47-52.

[17] E. Bauer and W. Wu, A hypoplastic constitutive model for cohesive powders. *Powder Technology* **85** (1995), 1-9.

[18] P. J. Olver, *Applications of Lie Groups to Differential Equations*. Springer-Verlag, New York 1986.